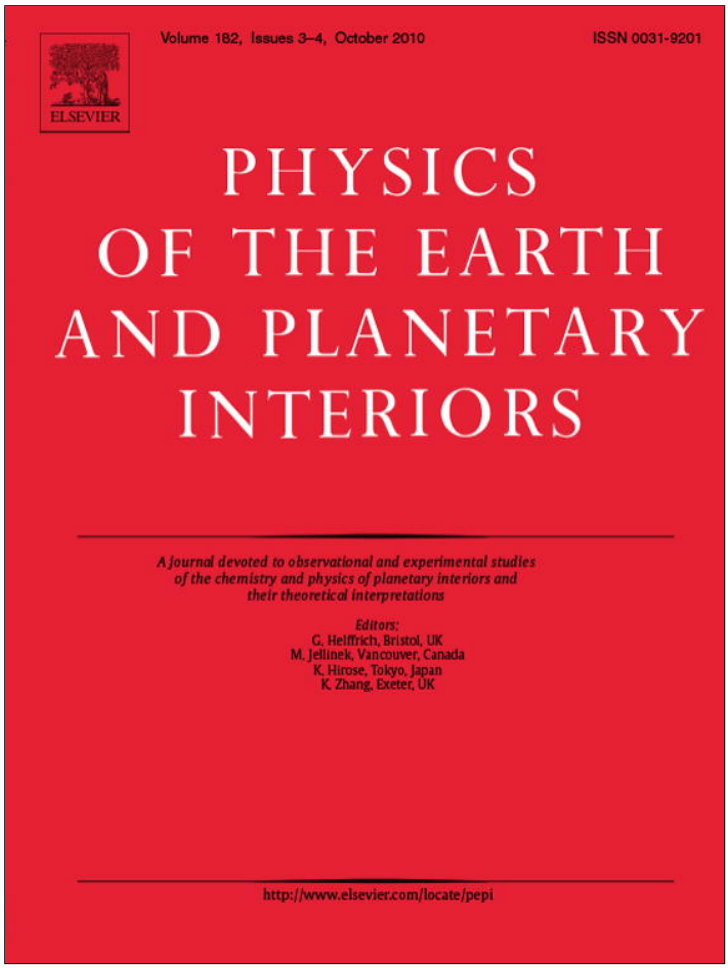

Physics of the Earth and Planetary Interiors 182 (2010) 139–151

Contents lists available at ScienceDirect

Physics of the Earth and Planetary Interiors

journal homepage: www.elsevier.com/locate/pepi

Dimensionality imprint of electrical anisotropy in magnetotelluric responses

A. Martí[a,*], P. Queralt[a], J. Ledo[a], C. Farquharson[b]

[a] Departament de Geodinàmica i Geofísica, Universitat de Barcelona, Spain
[b] Earth Sciences Department, Memorial University of Newfoundland, Canada

ARTICLE INFO

Article history:
Received 6 April 2010
Received in revised form 8 July 2010
Accepted 15 July 2010

Edited by: K. Zhang.

Keywords:
Magnetotellurics
Electrical anisotropy
Geoelectric dimensionality

ABSTRACT

Dimensionality analysis of magnetotelluric data is a common procedure for inferring the main properties of the geoelectric structures of the subsurface such as the strike direction or the presence of superficial distorting bodies, and enables the most appropriate modeling approach (1D, 2D or 3D) to be determined. Most of the methods currently used assume that the electrical conductivity of individual parts of a structure is isotropic, although some traces of anisotropy in data responses can be recognized. In this paper we investigate the imprints of anisotropic media responses in dimensionality analysis using rotational invariants of the magnetotelluric tensor. We show results for responses generated from 2D synthetic anisotropic models and for field data that have been interpreted as showing the effects of electrical anisotropy in parts of the subsurface structure. As a result of this study we extend the WAL dimensionality criteria to include extra conditions that allow anisotropic media to be distinguished from 2D isotropic ones. The new conditions require the analysis of the strike directions obtained and take into account the overall behavior of different sites in a survey.

1. Introduction

Electrical anisotropy in the Earth, caused by electrical conductivity varying with orientation, is a property that is increasingly being taken into account in the interpretation of magnetotelluric data. Electrical anisotropy in the crust can be caused by preferred orientations of fluids, sulfides or fractures (Wannamaker, 2005), whereas in the upper mantle, it is linked to the splitting of seismic SKS waves (Eaton and Jones, 2006), and is explained by either hydrogen diffusivity in olivine crystals (Wannamaker, 2005; Wang et al., 2006) or by the presence of partial melt elongated in the direction of plate motion (Yoshino et al., 2006).

Significant developments have been achieved regarding the study of electrical anisotropy using magnetotellurics. These deal with modelling and inversion schemes, which include anisotropy (Pek and Verner, 1997; Weidelt, 1999; Wang and Fang, 2001; Li, 2002; Yin, 2003; Pek and Santos, 2002, 2006), the analysis of magnetotelluric responses affected by anisotropy (Reddy and Rankin, 1975; Saraf et al., 1986; Osella and Martinelli, 1993; Heise and Pous, 2003; Heise et al., 2006), and the investigation of the intrinsic properties and processes causing electric anisotropy (Gatzemeier and Tommasi, 2006). Some of the aforementioned papers were published in a special issue dedicated to electrical and seismic continental anisotropy (Eaton and Jones, 2006). A review of earlier work can be found in Wannamaker (2005).

To date there have been no studies specifically discussing the effects of anisotropy on rotational invariants or its complete dimensionality characterization. The goal of this paper is to identify electrical anisotropy using dimensionality analysis based on the rotational invariants of the magnetotelluric tensor. Data were generated from various synthetic models with electrical anisotropy using the 2D code of Pek and Verner (1997). The results from a set of field data that has been interpreted as exhibiting the effects of anisotropic Earth structure (from the COPROD dataset) are also discussed.

2. Background

2.1. Dimensionality analysis in magnetotellurics

In the magnetotelluric (MT) method (e.g. Vozoff, 1991; Simpson and Bahr, 2005), dimensionality analysis is a common procedure for determining, prior to modeling, whether the measured data or computed responses (impedance tensor, Z; tipper, T; apparent resistivities, ρ_{ij}; and phases, φ_{ij}) at a given frequency (ω) correspond to 1D, 2D or 3D geoelectrical structures. It also allows identification and quantification of distortions (Kaufman, 1988; Groom and Bailey, 1989; Smith, 1995) and, when applicable, recovery of the directionality (strike) of the structures. Dimensionality analysis techniques search for particular relationships between the components of the magnetotelluric impedance tensor, $Z(\omega)$ (e.g. Cantwell,

* Corresponding author. Tel.: +34 934035913; fax: +34 934021340.
E-mail address: annamarti@ub.edu (A. Martí).

0031-9201/$ – see front matter © 2010 Elsevier B.V. All rights reserved.
doi:10.1016/j.pepi.2010.07.007

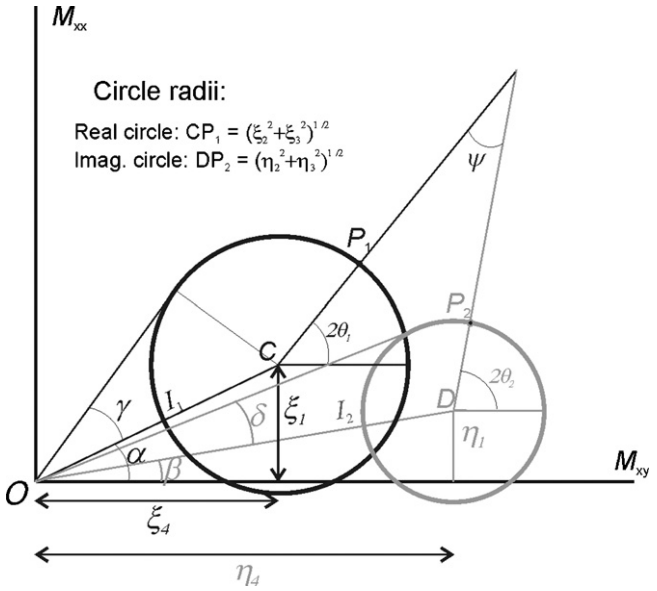

Fig. 1. Diagram of the real and imaginary Mohr circles generated after a complete rotation of the M_{xy} and M_{xx} components of the MT tensor. In black: parameters and circle associated with the real part. Grey: the equivalent for the imaginary part. After Lilley (1998a).

1960), or related functions, in order to identify each dimensionality type. Additional information can be obtained from the induction arrows (i.e., tipper vectors). The dimensionality analysis technique that sees the most widespread use is that of McNeice and Jones (2001). This technique uses the Groom and Bailey (1989) decomposition method to find the best fitting 2D parameters for a set of sites at different period bands. Lilley (1993) introduced the use of Mohr circles to display and analyze magnetotelluric data, allowing to distinguish their dimensionality and the presence of galvanic distortion. In two-dimensional cases, the regional geologic strike is estimated from either the real or imaginary parts of the magnetotelluric tensor (θ_{hr}, θ_{hq}, Eqs. (113) and (114), Lilley, 1998a). Lilley and Weaver (2009) presented a Mohr circles analysis for data with phases out of quadrant, although not particularly related with anisotropy.

Weaver et al. (2000) (based on Lilley, 1993, 1998a; Fischer and Masero, 1994 and Szarka and Menvielle, 1997) presented a complete dimensionality criteria based on the rotational invariants (WAL invariants) of the magnetotelluric tensor ($M(\omega)$, defined as the relationship between the electric field $E(\omega)$ and the magnetic induction $B(\omega)$; $M(\omega) = (1/\mu_0)Z(\omega)$). The WAL rotational invariants comprise seven independent (I_1, I_2, I_3, I_4, I_5, I_6 and I_7) parameters and one dependent (Q) parameter. They can be represented by Mohr circle diagrams (Lilley, 1993) (Fig. 1), and, except I_1 and I_2, they are taken as sines of angles, which implies an ambiguity in the quadrant to which each angle belongs. Also with the exception of I_1 and I_2, they are dimensionless and normalized to unity, with their vanishing having a physical interpretation that is related to the geoelectric dimensionality (see Weaver et al., 2000, for a full description of the invariants).

WAL dimensionality criteria, based on the vanishing or not of some of the invariants (I_3–I_7), are summarized in Table 1. Dimensionality analysis using WAL criteria has been implemented, including data errors and band averages (Martí et al., 2004), in the WALDIM code (Martí et al., 2009). Given that on field, therefore noisy data, the invariants are rarely precisely zero, the program uses two threshold values (as suggested by Weaver et al., 2000): τ, for I_3–I_7; and τ_Q, for invariant Q; below which the invariants are taken to be zero.

It is also important to note the parameters that can be derived from the invariants for specific dimensionality cases: In 1D cases, invariants I_1 and I_2 provide information about the 1D magnitude and phase of the geoelectric resistivity (ρ_{1D} and φ_{1D}). In 2D, the strike angle (referred to as θ_{2D}) can be obtained from the real and imaginary parts of the MT tensor, with θ_1 and θ_2 giving the same value for the strike angle (see expressions in the Appendix A). In 2D cases affected by galvanic distortion (identified as 3D/2D), the strike angle ($\theta_{3D/2D}$) is computed considering both the real and imaginary parts of the MT tensor and the distortion parameters, as ϕ_1 and ϕ_2 (Smith, 1995), which are linear combinations of the Groom and Bailey (1989) twist and shear angles ($\varphi_t = \phi_1 + \phi_2$, and $\varphi_e = \phi_1 + \phi_2$). In 2D cases (which are particular cases of 3D/2D), the strikes computed as θ_1, θ_2 and $\theta_{3D/2D}$ (see Appendix A) are equivalent and the values of φ_t and φ_e are negligible.

It must be remembered that the WAL criteria, as well as the other dimensionality analysis methods, are based on the assumption that the geoelectrical structures are isotropic.

Another tool used to infer the dimensionality in isotropic media is the phase tensor (Caldwell et al., 2004), which is not affected by galvanic distortion (hence only 1D, 2D and 3D cases can be identified). It can be represented by an ellipse, characterized by 4 parameters, the 3 rotational invariants Φ_{max}, Φ_{min} (principal directions) and β, and the non invariant angle α (see Caldwell et al., 2004, for a more detailed description). In 1D cases, the ellipses are circles ($\Phi_{max} = \Phi_{min}$). In 2D, Φ_{max} and Φ_{min} have different values, α indicates the strike direction and β is null. In 3D, β is non-zero. Heise et al. (2006) used the phase tensor diagrams to represent the responses of models with electric anisotropy. We will compare the phase tensor analysis with the WAL dimensionality criteria for some of the examples presented below.

2.2. Electrical anisotropy and modelling

The properties of an anisotropic medium need to be expressed in a tensor form. For the case of electrical anisotropy, the conductivity (σ, reciprocal of the resistivity ρ, $\sigma = 1/\rho$) adopts the general form of a symmetric tensor with non-negative components,

$$\sigma = \begin{bmatrix} \sigma_{xx} & \sigma_{xy} & \sigma_{xz} \\ \sigma_{yx} & \sigma_{yy} & \sigma_{yz} \\ \sigma_{zx} & \sigma_{zy} & \sigma_{zz} \end{bmatrix}, \quad (1)$$

where x (North), y (East) and z (vertically downwards) are the orthogonal axes of a Cartesian coordinate system. The conductivity tensor can represent an intrinsic property of the material (microscopic anisotropy) (Negi and Saraf, 1989), or it can represent the result of mixing in a preferred orientation of two or more media with differing conductivities (macroanisotropy) (e.g. Wannamaker, 2005). The resolving power of the MT method and the depths at which anisotropic media are typically located (lower crust, upper mantle), usually make it impossible to distinguish between them (Weidelt, 1999).

Using Euler's elementary rotations the conductivity tensor can be diagonalised and its principal directions obtained, namely the strike, dip and slant anisotropy angles (α_S around z-axis, α_D around x'-axis and α_L around z''-axis) (Fig. 2). Hence, the conductivity tensor can be specified by six parameters: the three conductivity components along the principal directions (σ'_{xx}, σ'_{yy} and σ'_{zz}) and their corresponding angles.

Particular cases of anisotropy, specified in terms of the relationships between the components along the principal directions of the conductivity tensor, are azimuthal anisotropy ($\sigma'_{xx} = \sigma'_{zz}$ or $\sigma'_{yy} = \sigma'_{zz}$, anisotropy in only one direction, x or y) and uniaxial anisotropy ($\sigma'_{xx} = \sigma'_{yy} \neq \sigma'_{zz}$). In the latter,anisotropy can only be

Table 1
Dimensionality criteria according to the WAL invariant values of the magnetotelluric tensor (modified from Weaver et al., 2000). Row "2D" with the grey background is extended in Table 3 where structures with anisotropy are considered.

Case	I_3 to I_7 and Q values	GEOELECTRIC DIMENSIONALITY
1	$I_3 = I_4 = I_5 = I_6 = 0$	**1D** $\rho_{1D} = \mu_0 \frac{\left(I_1^2 + I_2^2\right)}{\omega}$, $\varphi_{1D} = \arctan\left(\frac{I_2}{I_1}\right)$
2	$I_3 \neq 0$ or $I_4 \neq 0$; $I_5 = I_6 = 0$; $I_7 = 0$ or Q = 0 ($\xi_4 \neq 0$ and $\eta_4 \neq 0$)	**2D**
3a	$I_3 \neq 0$ or $I_4 \neq 0$; $I_5 \neq 0$; $I_6 = 0$; $I_7 = 0$	**3D/2Dtwist** 2D affected by galvanic distortion (only twist)
3b	$I_3 \neq 0$ or $I_4 \neq 0$; $I_5 \neq 0$; $I_6 = 0$; Q = 0	**3D/1D2D** Galvanic distortion over a 1D or 2D structure (non-recoverable strike direction)
3c	$I_3 \neq 0$ or $I_4 \neq 0$; $I_5 = I_6 = 0$; $I_7 = 0$ or Q = 0 ($\xi_4 = 0$ and $\eta_4 = 0$)	**3D/1D2Ddiag** Galvanic distortion over a 1D or 2D structure resulting in a diagonal MT tensor
4	$I_3 \neq 0$ or $I_4 \neq 0$; $I_5 \neq 0$; $I_6 \neq 0$; $I_7 = 0$	**3D/2D** General case of galvanic distortion over a 2D structure
5	$I_7 \neq 0$	**3D** (affected or not by galvanic distortion)

identified by the vertical component of the electric and magnetic fields (Negi and Saraf, 1989).

For anisotropic media, the MT forward problem must be solved, in general, using a numerical approach. The code of Pek and Verner (1997) uses the finite-difference method to obtain the responses for 1D and 2D anisotropic media.

The magnetotelluric responses obtained from an anisotropic medium are characterized by resistivity shifts, phase splits (which are related to anisotropy contrasts rather than bulk anisotropy of the medium Heise et al., 2006), and induction arrows not correlated to the principal direction indicated by the MT tensor (Pek and Verner, 1997; Weidelt, 1999).

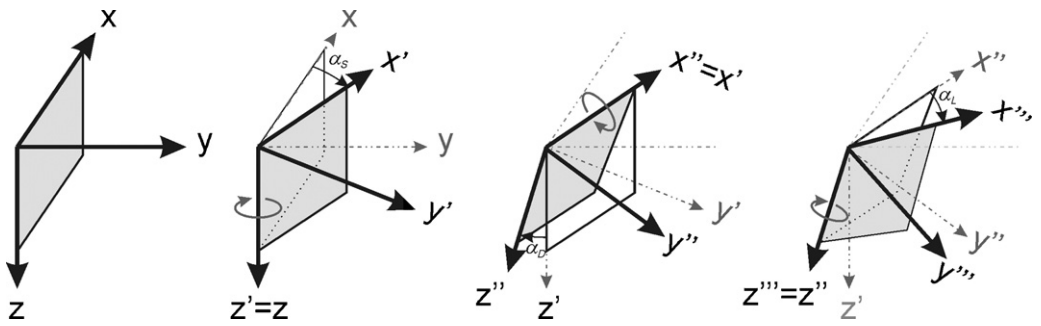

Fig. 2. Diagram of successive Euler rotations applied to generate any orientation of the anisotropic principal directions, using the anisotropy strike (α_S), dip (α_D) and slant (α_L) angles.

Table 2
Resistivity values and orientations of the three anisotropic half-space models **1a**, **1b** and **1c**.

Homogeneous models $\rho'_{xx} = 50\,\Omega$ m and $\rho'_{yy} = \rho'_{zz} = 500\,\Omega$ m	Anisotropy angles
Model 1a	$\alpha_S = 0^\circ$, $\alpha_D = 0^\circ$, $\alpha_L = 0^\circ$
Model 1b	$\alpha_S = 40^\circ$, $\alpha_D = 0^\circ$, $\alpha_L = 0^\circ$
Model 1c	$\alpha_S = 0^\circ$, $\alpha_D = 55^\circ$, $\alpha_L = 20^\circ$

3. Dimensionality analysis of synthetic anisotropic model responses using WALDIM

In this section we present some examples for synthetic models with anisotropy, the responses of which have been calculated using the code of Pek and Verner (1997). In these, we have performed the dimensionality analysis using the WALDIM code and we have analyzed the results indicating which features are characteristic of the anisotropic structures.

The models were chosen to increase gradually in complexity starting from the most simple. Only 2D situations, not 3D situations, are considered in this study as it is not possible to separate the imprint of anisotropy from 3D effects.

Except when indicated, all the models have dimensions of 860 km (y, towards East) by 186 km (z, vertical downwards), and are discretised using 40 (y) by 30 (z) cells, plus 11 air layers. The responses were computed at each surface node, at the periods indicated in the sections below, following the e^{+iwt} convention for the time-harmonic factor of the electric and magnetic fields. WALDIM analysis was performed for each resulting MT tensor, with 1% random noise having been added to each component. Threshold values of $\tau = 0.1$ and $\tau_Q = 0.1$, which were tested to be consistent with the noise level applied, were used. We also tested, by representing the results using Mohr circle diagrams (following Lilley, 1998b), that the invariant values are obtained as sines of positive angles within the range 0–90°; and that the dimensionality description obtained from the invariant parameters and Mohr circles are consistent.

3.1. Anisotropic half-space

For the simplest cases, we considered three models consisting of anisotropic half-spaces.

The three models have azimuthal anisotropy with the same resistivity values, $\rho'_{xx} = 50\,\Omega$ m and $\rho'_{yy} = \rho'_{zz} = 500\,\Omega$ m, and are distinguished from each other by the orientation of the principal directions. In the first model (**1a**), these coincide with the measurement axes. In the second (**1b**), these have been rotated through a strike angle $\alpha_S = 40^\circ$ around the z axis. In the third model (**1c**), a general rotation using dip (55°) and slant (20°) angles has been considered (see Table 2). The responses for each model were computed at $T = 1$ s, 3.2 s, 10 s, 32 s, 100 s and 320 s.

For the three models, the responses are site independent, and only show slight variations with period due to numerical inaccuracies. Apparent resistivity values depend on the projection of the anisotropy direction on to the x and y axes, as shown in Fig. 3(a). Phase values (not shown in the figure) of the off-diagonal

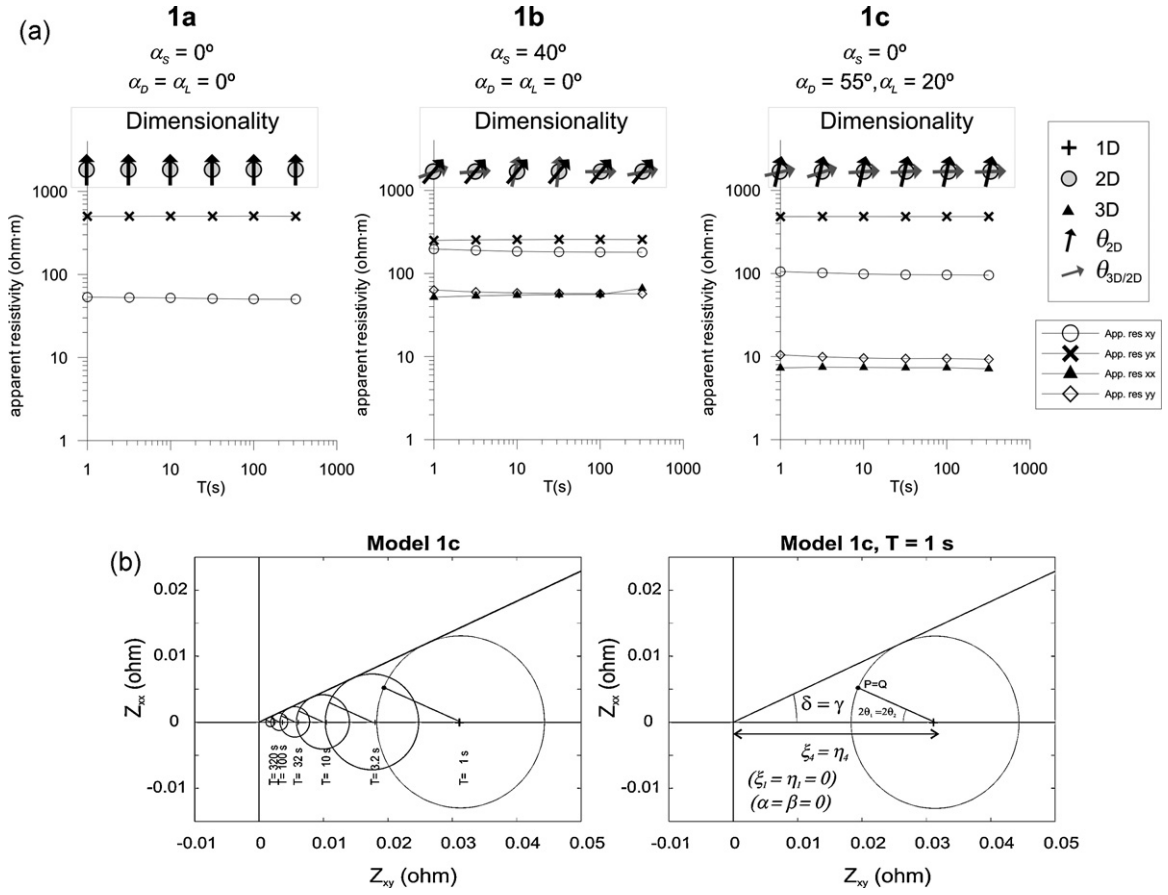

Fig. 3. (a) Dimensionality and apparent resistivity responses for the three anisotropic half-space models (**1a**, **1b** and **1c**), at one single site (located at the centre of the model) for the computed periods. Strike directions are shown assuming a 2D structure (θ_{2D}) and assuming galvanic distortion over a 2D model ($\theta_{3D/2D}$) (except at model **1a** where the two directions are coincident). *xx* and *yy* apparent resistivities in model **1a** are null and hence not shown. (b) Left: Mohr diagram for the responses of model **1c**. Both real and imaginary circles are coincident and agree with a 2D structure. Right: Mohr diagram for a single period, $T = 1$ s, of model **1c** showing the main parameters, and the strike angles θ_1 and θ_2 (coincident with θ_h, Eqs. (113) and (114) in Lilley, 1998a). Note that $\theta_{3D/2D}$ cannot be represented using Mohr circles.

components are 45° (*xy* polarization) and −135° (*yx* polarization) (as expected from a medium without vertical variations in resistivity). For model **1a**, *xx* and *yy* apparent resistivities are zero, and hence, the corresponding phases are undetermined. In contrast, for models **1b** and **1c**, *xx* and *yy* phases are 45° and −135° respectively. These responses, observed at a particular site, could be interpreted as a case of galvanic distortion (with shear and anisotropy effects) over a homogeneous medium.

Regarding the dimensionality analysis results, invariant values present similar relationships for the three models, for all sites and frequencies: $I_3 = I_4 > \tau$, I_5 and $I_6 < \tau$ and $Q < \tau_Q$. The exception is I_7, with values either below or above the threshold value, due to random noise effects. The WAL criteria define the dimensionality as 2D for all models (Fig. 3(a)) and the strike directions are well defined: $\theta_1 \approx \theta_2$ (=θ_{2D}), with small errors, also due to the noise added. For models **1a** and **1b**, these angles are coincident with α_S (0° or 40° respectively), and for model **1c** it is 12°, due to the projection onto the horizontal plane of the new x' and y' axes, resulting from the dip and slant rotations. The dimensionality and the strike direction also agree with the Mohr diagrams ($\theta_{hr} \approx \theta_{hq} \approx \theta_1 \approx \theta_2 = 12°$), as shown for model **1c** in Fig. 3(b).

For models **1b** and **1c**, for which the anisotropy directions are not aligned with the measuring axes, two particular features are observed: $\theta_{3D/2D}$ values (which cannot be represented using Mohr circles) are unstable and are different from θ_{2D} (Fig. 3(a)). This does not happen in isotropic 2D structures. In the Appendix A, the analytical expressions used to obtain the strike directions for the magnetotelluric tensors corresponding to a 2D isotropic model and an anisotropic half-space are developed. In the anisotropic case, the value of $\theta_{3D/2D}$ is indeterminate, but in the responses of the synthetic model its values are unstable due to the effects of the noise. The main result is that both the analytic expressions and the responses prove that θ_{2D} and $\theta_{3D/2D}$ are not coincident in the case of an anisotropic half-space.

For the three models, phase tensors (Caldwell et al., 2004; Heise et al., 2006) would be represented by unit circles independent of the orientation of the principal directions, and would thus provide no hint of anisotropy.

In model **1a**, the fact that all site responses are the same whilst the dimensionality is 2D indicate that either all the measuring sites are aligned with the strike direction or that the structure is not isotropic but anisotropic. Hence, when the anisotropic directions are coincident with the measuring axes, the responses do not allow the presence of anisotropy in a half-space to be distinguished. In contrast, when anisotropy is not aligned with the measuring axes (models **1b** and **1c**), the non agreement between the values of the strike directions θ_{2D} and $\theta_{3D/2D}$ is an indication that the half-space over which the measurements are obtained is indistinctly anisotropic. This is an important result, given that it is common to state that 1D anisotropic media are indistinguishable from 2D isotropic media. This type of anisotropic structure cannot be identified using the phase tensor.

3.2. 1D media with one and two anisotropic layers

The first one-dimensional model presented here (model **2a**) was taken from one of the examples provided with the Pek and Verner (1997) code. It consists of a layered structure with an embedded anisotropic layer (Fig. 4): ($\rho'_{xx} = 1\,\Omega$ m and $\rho'_{yy} = \rho'_{zz} = 100\,\Omega$ m, and $\alpha_S = 30°$, $\alpha_D = 0°$, $\alpha_L = 0°$). The model responses were computed at 10 periods between $T = 1$ s and $T = 32{,}000$ s.

The MT responses, which are shown in Fig. 4, are the same at all sites. Diagonal responses are coincident ($xx = yy$), whereas the off-diagonal responses show a split between the polarizations. The off-diagonal resistivity and phases are plotted together with the responses ($xy = yx$) of two models in which the anisotropic layer is replaced with an isotropic one; the first model with a 1 Ω m layer, and the second with a 100 Ω m layer (Fig. 4). Because of the rotation

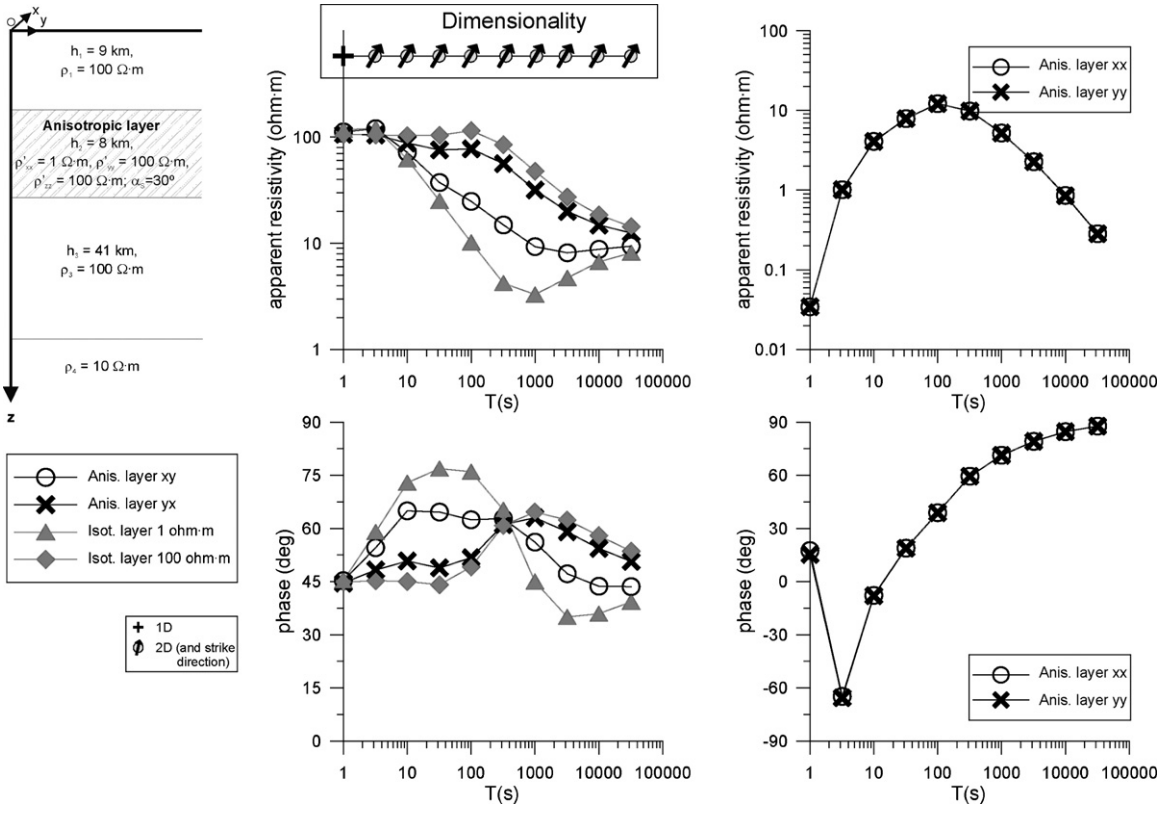

Fig. 4. Cross-section of model 2a, corresponding to a layered model with an anisotropic layer, and resistivity and phase responses obtained at any site of the model. The off-diagonal resistivity and phases are plotted together with the responses of a model with an isotropic layer of 100 Ω m and a model with an anisotropic layer of 1 Ω m.

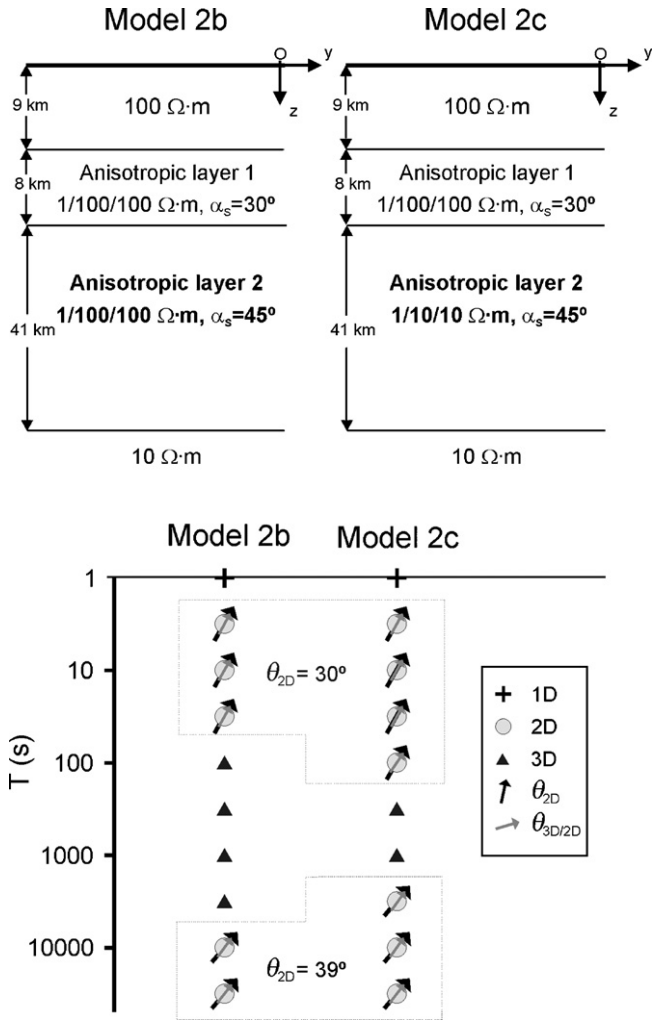

Fig. 5. Top: Cross-sections of models **2b** and **2c**, consisting of 1D models with two anisotropic layers. Bottom: Dimensionality pattern of the corresponding responses, with the principal angles and distortion angles indicated.

(α_S) of the principal directions, the values of the off-diagonal resistivities and phases for the model with the anisotropic layer are smoother than those for the models with the isotropic layers.

The WAL dimensionality criteria ($I_3 = I_4 > \tau$, I_5, I_6 and $I_7 < \tau$ and $Q > \tau_Q$) indicate 2D structures with $\theta_{2D} = 30^\circ$ ($=\alpha_S$) for all periods (Fig. 4), except for $T = 1$ s at which the criteria indicate 1D structure because the skin depth (5 km) is smaller than the top of the anisotropic layer. For the periods at which 2D structure is indicated, the strike direction computed as $\theta_{3D/2D}$ is coincident with θ_{2D} and the distortion parameters are practically null.

The effects of the inclusion of a second anisotropic layer just below the first one were also investigated by considering the third layer of model **2a** to be anisotropic as well. In the first of these models (model **2b**), this new anisotropic layer has the same resistivity values as the upper one, but with the main directions rotated at an angle $\alpha_S = 45^\circ$. In the second model (model **2c**), both the resistivity values ($\rho'_{xx} = 1\,\Omega$ m and $\rho'_{yy} = \rho'_{zz} = 10\,\Omega$ m) and α_S (45°) were changed in the new layer. The dimensionality pattern for both (Fig. 5) is, from the shortest to the longest period: 1D (corresponding to the first isotropic layer), 2D with a 30° strike direction (corresponding to the first anisotropic layer), 3D (due to an abrupt increase in the value of invariant I_7 caused by the inclusion of the second anisotropic layer), and finally 2D, with an approximately 39° strike, a value in between the two anisotropy strike values of the two layers (30° and 45°). In all the 2D cases, as had happened in the case with a single anisotropic layer, the directions θ_{2D} and $\theta_{3D/2D}$ are coincident.

We can summarize that in a 1D medium with one anisotropic layer, dimensionality is 2D with a well defined angle θ_{2D} (equivalent to α_S, or a projection of the anisotropic directions onto the horizontal if other rotations have been performed), which has the same value as $\theta_{3D/2D}$, as would happen in an isotropic medium. In this case the only hint that anisotropy is present is the fact that the responses are the same at all sites, except when the anisotropy angle is 0°, for which responses are equivalent to those of a 2D model with measurements along the strike direction. When two different anisotropic layers are considered, the dimensionality varies with period: from 2D (corresponding to the first anisotropic layer), to 3D, and back to 2D.

3.3. 2D anisotropic media

In this section, we considered two groups of models based on the examples used in Reddy and Rankin (1975) and Heise et al. (2006). The first group contains models in which the electrical properties vary only in the horizontal direction; the models in the second group possess more general two-dimensional variations.

3.3.1. Anisotropic dyke

The models in the first group (Fig. 6) consist of a vertical dyke intruded into a medium with differing electrical properties. Initially we consider a model in which both the dyke and the surroundings are isotropic (model **3a**, $\rho_{\text{dyke}} = 10\,\Omega$ m and $\rho_{\text{surroundings}} = 100\,\Omega$ m). A second model (model **3b**) consists of an anisotropic dyke ($\rho'_{xx} = 3\,\Omega$ m, $\rho'_{yy} = 10\,\Omega$ m, $\rho'_{zz} = 20\,\Omega$ m, and $\alpha_S = 30^\circ$, $\alpha_D = 0^\circ$, $\alpha_L = 0^\circ$) sandwiched by an isotropic medium of $\rho = 100\,\Omega$ m. In the third model, both the dyke and the surroundings are anisotropic. The responses for the three models were computed at one period per decade between $T = 1$ s and $T = 10{,}000$ s.

For the isotropic model, **3a**, the dimensionality is 1D at sites located outside and far from the dyke (Fig. 6(a)). Inside and surrounding the dyke, the dimensionality is 2D (0° strike), except at the first periods for the sites located at the centre of the dyke for which the dimensionality is 1D. At these periods these sites are too far from, and hence not affected by, the dyke boundaries.

For model **3b** (anisotropic dyke surrounded by an isotropic medium), the dimensionality pattern outside the dyke is similar to that of model **3a** (Fig. 6(b)): mainly 1D and 2D (with 0° strike). At the edges of the dyke and at the longest periods the dimensionality is 3D/1D2D. For sites located over the dyke is the dimensionality is 3D, except for the shortest periods at the central part, for which the dimensionality is 2D with a strike of 30°. In these 2D cases, the strike direction is coincident with the anisotropy angle α_S. However, the direction given by $\theta_{3D/2D}$ has a different value (60°) from that of θ_{2D} (30°), in contrast to what was observed for the anisotropic half-space models (models **1b** and **1c**), and the distortion parameters are not negligible ($\varphi_t = 2^\circ$ and $\varphi_e = -14^\circ$).

When both the dyke and surroundings are anisotropic (model **3c**), the dimensionality is more complex. Nevertheless there are clear differences with the results observed for the previous models **3a** and **3b**, and there are distinctive features associated with each region of the model (Fig. 6(c)). Outside the dyke and far from its edges the dimensionality is 2D with $\theta_{2D} = 55^\circ$, which is different from the value given by $\theta_{3D/2D}$ (with variable values, as shown in Fig. 6(c)). Still outside but closer to the dyke edges, the dimensionality is mainly 3D/2D with a strike direction of around 75° or 80° and distortion parameters φ_t negligible and $\varphi_e = -10^\circ$. At the edges, the dimensionality is either 3D/2D or 3D/1D2D. The 3D/2D cases obtained both outside the dyke and at the edges have the peculiarity that, according to the invariant parameters, the dimensionality should be 2D, but the strike directions are inconsistent ($\theta_1 \neq \theta_2$).

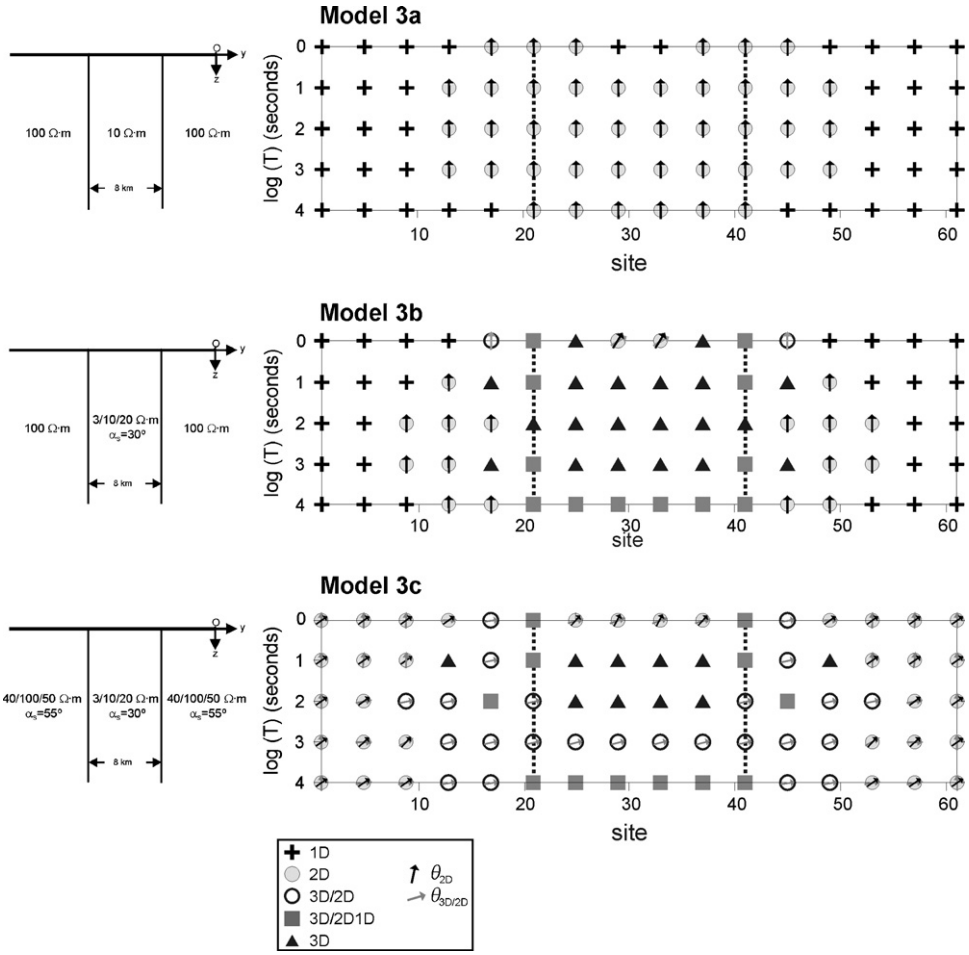

Fig. 6. Cross-section of models **3a**, **3b** and **3c** and the corresponding dimensionality patterns. Only one out of every 4 sites is plotted. For model **3a**, in the 2D cases, the strike angle is 0°.

It would therefore not be possible to rotate and obtain a regional 2D tensor. Instead, the impedance tensor is better described as 3D/2D with the $\theta_{3D/2D}$ strike and distortion angles that are small but not negligible (Martí et al., 2009). The use of these strike and distortion angles allows, in isotropic structures, the decomposition of the impedance tensor to be performed and a 2D tensor recovered. Inside the dyke, at the shortest period, the dimensionality is 2D, with $\theta_{2D} = 30^\circ = \alpha_S$, inconsistent with $\theta_{3D/2D}$ (70°), and with non-negligible values of the shear distortion angle ($\varphi_e = -10^\circ$). As the period increases, the dimensionality becomes 3D, 3D/2D (with $\theta_{3D/2D} = 75^\circ$, $\varphi_t = -12^\circ$ and $\varphi_e = -10^\circ$), and finally 3D/1D2D.

From the above dimensionality description, the presence of anisotropy can be recognized in the 2D cases, for which the strike directions given by θ_{2D} (which agree with the anisotropic azimuth) and $\theta_{3D/2D}$ are different (Fig. 6). Moreover, there are also cases that should be 2D according to the invariants, but for which $\theta_1 \neq \theta_2$. Therefore, these cases are described as 3D/2D, with the strike direction ($\theta_{3D/2D}$, computed from the real and imaginary parts of the tensor) close to the sum of both anisotropic directions (80°). θ_{hr} and θ_{hq} do not provide the correct strike direction either, as they are computed using the real or the imaginary parts separately. Also, for sites over the dyke and at the edges, some 3D/1D2D and 3D cases are obtained.

3.3.2. 2D conductive bodies and an anisotropic layer

The second set of models is taken from the 2D examples used in Heise et al. (2006). This set explores phase splits in responses from anisotropic structures, and the identification of anisotropy using phase information (in particular, the phase tensor).

Model **4a** contains an anisotropic layer (with main directions along the *x*, *y* and *z* axes) and two conductive blocks. Model **4b** is isotropic and contains two conductive blocks similar to those in model **4a** (Fig. 7). Heise et al. (2006) show how both models give similar phase tensor and induction arrow responses, except at the longest periods, where the induction arrows for the isotropic model are significant, whereas in the anisotropic model they are almost null.

Rotational invariants and dimensionality of the responses of these two models were computed between 1 s and 30,000 s (Fig. 8). The invariants have similar values for both models, and hence the dimensionality displays similar patterns for both models. In general, the dimensionality is 1D for periods up to approximately 100 s, and 2D for the rest. However, the dimensionality of the first and last sites, located on top of the conductive blocks, is different for each model. For model **4a** dimensionality is 1D up to 100 s, then becoming 2D as a consequence of the directionality introduced by the anisotropic layer, affecting all sites. For model **4b** all the cases are 1D as these sites are not affected by the lateral contrasts at the limits of the two conductive bodies. The phase tensor ellipses, which were computed for both models for the first site, also show this difference between the two models (Fig. 9). These results confirm that for 2D models with anisotropic structures aligned with the main directions, both the invariants and the phase tensor provide the same information, and that for this example they cannot distinguish between the anisotropic and isotropic models.

Additionally, we considered model **4a** and modified the anisotropic layer by applying a rotation of the principal directions ($\alpha_S = 30^\circ$). The dimensionality of the responses of the resulting

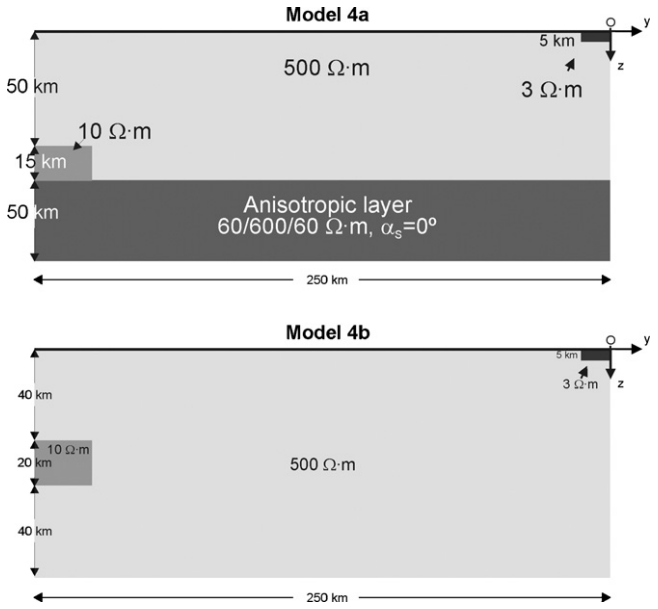

Fig. 7. Cross-sections of models **4a** and **4b** (from Heise et al., 2006), used to compute the responses from general 2D models with anisotropic structures.

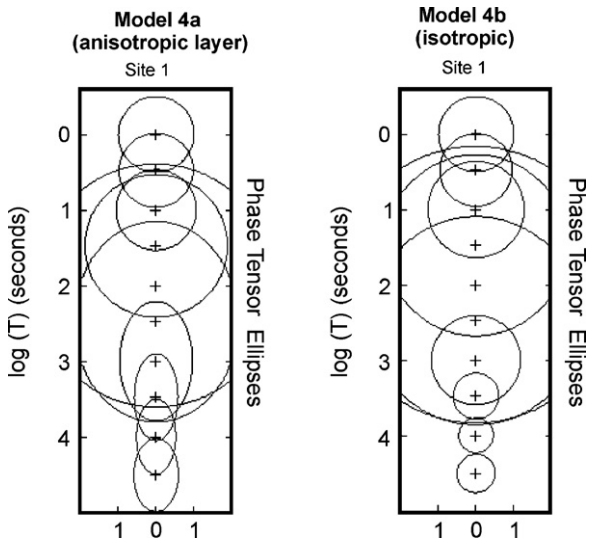

Fig. 9. Phase tensor diagrams corresponding to site 1 (located at 0 km) for models **4a** and **4b**. The horizontal axis indicates the value of the phase tangent. These diagrams are very similar to those obtained for the last site (site 33, located at 250 km).

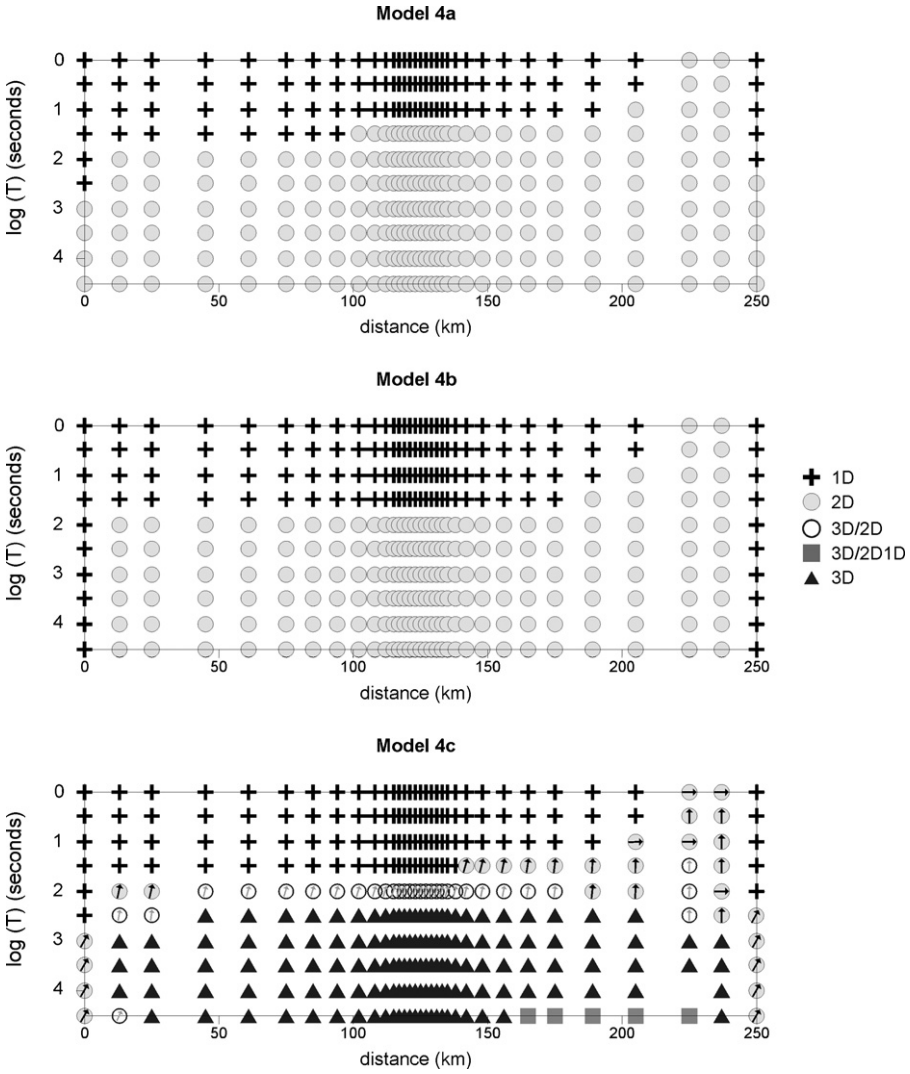

Fig. 8. Dimensionality patterns corresponding to the responses of models **4a** and **4b** and **4c**. All sites where responses have been computed are shown. Blank zones inside the diagrams correspond to cases for which none of the defined criteria were met and hence for which the dimensionality could not be determined.

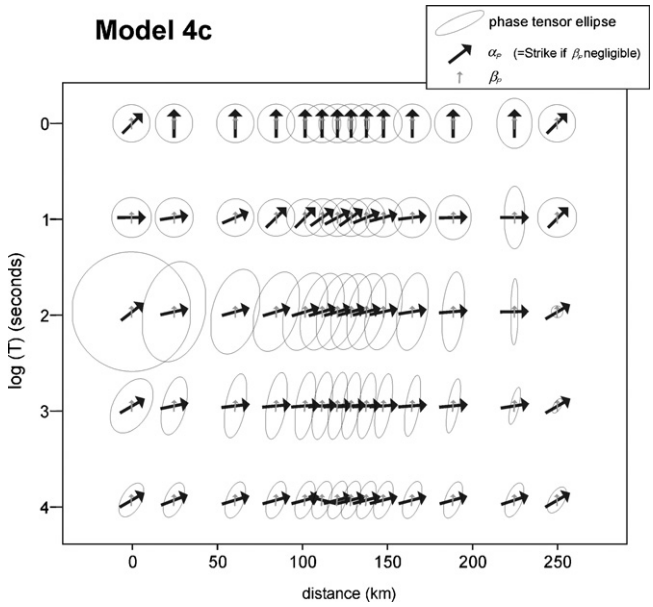

Fig. 10. Phase tensor diagrams corresponding to the responses of model **4c**, for 5 periods between 1 s and 10,000 s. One out of every two sites is shown, except between 100 km and 150 km, where only one out of every 4 sites is represented. The minor and major axes of the ellipses indicate the value of the phase tangent in the way that the radii of the circles at 1 s are equal to 1.

model, identified as **4c**, is shown in Fig. 8(c). The dimensionality pattern is significantly more complex than for the previous models. Up to 100 s, the dimensionality is similar to that of models **4a** and **4b** (mostly 1D with 2D cases at the rightmost side of the model due to the shallow conductive structure). For periods around 100 s, most of the 1D cases become 2D (θ_{2D} being consistent with $\theta_{3D/2D}$) or 3D/2D (with an approximately 15° strike). At longer periods, the general trend is that the cases that were 1D and 2D in models **4a** and **4b** become 2D and 3D, respectively; with some 3D/2D and 3D/1D2D exceptions. In all 3D/2D cases (most of them at 100 s), as happened for the model with the anisotropic dyke (**3c**), invariant values indicate 2D dimensionality, but, given that the two strike directions, θ_1 and θ_2, are significantly different, the impedance tensor is better described as 3D/2D with $\theta_{3D/2D}$. This observation is a clear indication of the presence of anisotropy in the structures, with anisotropic directions non-aligned to the principal structural directions. In the phase tensor diagrams of these model responses (Fig. 10) an equivalent effect can be observed at 100 s: the values of β are negligible (note that only angle values lower than 3° are considered negligible), whereas the main directions of the ellipse differ significantly from the strike angle α.

Hence, for 2D models, both the WALDIM criteria and the phase tensor diagrams are able to identify the presence of anisotropic structures with principal directions not coincident with the measuring axes.

4. Anisotropy in field data: the COPROD dataset

In this final section we refer to one case of field data that has been associated with anisotropy. This is the well known COPROD2 dataset, from southern Saskatchewan and Manitoba (Canada), which revealed the presence of the North American Central Plains conductivity anomaly (NACP) (Jones and Craven, 1990; Jones et al., 1993). This dataset was used to test inversion codes (see Jones, 1993). Some of the 2D models that were obtained consisted of multiple isotropic high conductivity bodies separated by resistive regions. Jones (2006) revisited the data and, using one of the sites on top of the NACP anomaly as a reference (85_314), proposed a 2D anisotropic model. This model consists of a thin superficial conductive layer (3 Ω m), a 100 km thick lithosphere of 1000 Ω m, in which a single anisotropic block ($\rho'_{xx} = 0.5\,\Omega$ m along strike, $\rho'_{yy} = \rho'_{zz} = 1000\,\Omega$ m) is embedded, and a basal conducting layer of 10 Ω m. The off-diagonal responses for this model are in good agreement with those of the observed data, reproducing the split between TE and TM modes.

We computed the dimensionality for the synthetic tensors of the sites located over the anisotropic body. We obtained 1D cases, and 2D cases with 0° strike (anisotropy aligned with the measuring directions) (Fig. 11(a)).

The data for site 85_314 was used by Martí et al. (2009) as an example for dimensionality analysis using the WALDIM code. Up

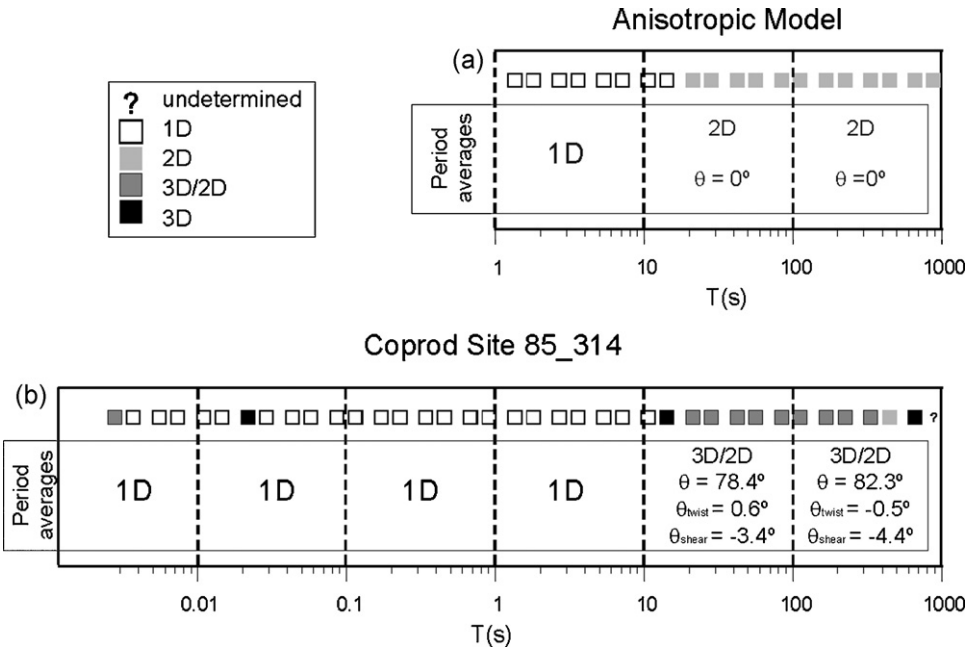

Fig. 11. Dimensionality cases for: (a) the responses of the anisotropic model presented by Jones (2006), which fits the off-diagonal components of site 85_314 in the COPROD2 dataset; and (b) for all the components of site 85_314 from the COPROD2 dataset (modified from Martí et al., 2009).

Table 3
Dimensionality criteria extended to anisotropic structures, characterized by the WAL invariants criteria indicating isotropic 2D.

I_3 to I_7 and Q	GEOELECTRIC DIMENSIONALITY ("2D cases")			
$I_3 \neq 0$ or $I_4 \neq 0$; $I_5 = I_6 = 0$; $I_7 = 0$ or Q = 0	$\theta_{2D} = \theta_1 = \theta_2 = \theta_{3D/2D}$	Identical tensors at all sites (period dependent)	$\theta_{2D} = 0$	1D MEDIUM WITH ONE ANISOTROPIC LAYER or 2D ISOTROPIC MEDIUM WITH MEASUREMENTS ALONG STRIKE
			$\theta_{2D} \neq 0$	1D MEDIUM WITH ONE ANISOTROPIC LAYER
		Different tensors at each site (period dependent)		2D ISOTROPIC MEDIUM
	$\theta_{2D} \neq \theta_{3D/2D}$	Identical tensors at all sites (period independent)		HOMOGENEOUS ANISOTROPIC MEDIUM
	$\theta_{2D} \neq \theta_{3D/2D}$ or $\theta_1 \neq \theta_2$	Different tensors at each site (period dependent)		ANISOTROPIC STRUCTURE IN A 2D MEDIUM

to 10 s, the data can be described as 1D. At periods longer than 10 s invariant values indicate 2D. However, at these periods strike angles θ_1 and θ_2 differ significantly, and hence the data were better described as 3D/2D, with a strike direction around 80° and small twist and shear distortion angles (lower than 5°) (Fig. 11(b)). This allowed 2D regional tensors to be obtained from tensor decomposition. According to the tests presented here, the discrepancy between the dimensionality descriptions from the model with the anisotropic block and the field data lies in the fact that in the synthetic data all the diagonal responses are null, whereas in the field data the values of the diagonal components, especially for the longest periods, are significant.

From our new characterization of anisotropy in dimensionality analysis, it is clear that the dimensionality of site 85_314 is compatible with a 2D model that contains at least one anisotropic block or layer, having anisotropy directions aligned with the strike indicated in the dimensionality analysis (in this case of around 80°). Hence, if the anisotropic block modeled by Jones (2006) had an anisotropic azimuth of 80°, the invariant values of the responses would correspond to 2D structures with two different strike directions θ_1 and θ_2. This would be in agreement with the observed data.

5. WAL criteria extended to accommodate anisotropy

The results obtained from this study have allowed specific relationships to be established between the invariants and strike directions that are linked to the presence of anisotropy. In general, these conditions are not recognized from a single tensor alone, but from the pattern at different sites and periods. The main imprint of anisotropy can be seen in the 2D cases (according to WAL isotropic criteria), with strike directions that are not consistent, or relationships between tensors that would not correspond to isotropic structures. In these cases, the strike obtained is related to the orientation of the anisotropy rather than to the structural direction. Table 3 contains the new dimensionality criteria extended to accommodate these cases with anisotropy and to distinguish them from isotropic two-dimensionality: anisotropic half-space, a 1D medium with one anisotropic layer, and an anisotropic 2D medium.

However, it must be remembered that it is not always possible to identify anisotropy when the main directions are aligned with the measuring axes, or to retrieve all the parameters that characterize anisotropy from the observed responses and the dimensionality analysis alone.

Table 3 considers the dimensionality observed in a particular tensor. In particular situations described in the text, some patterns can be observed such as that of a 1D model with two anisotropic layers (2D, 3D and 2D cases, as the period increases).

Hence, once the dimensionality of the full dataset is obtained (it is recommended to plot dimensionality maps), one should check for anisotropic imprints and patterns as described in the text, and evaluate what type of anisotropic media might exist beneath the survey area.

6. Conclusions

The most important contribution of this study is the demonstration that it is possible to identify the presence of anisotropy in the dimensionality description given by the WAL criteria. In addition, we have extended the WAL invariants criteria to differentiate anisotropic from isotropic media. Hence, when assessing the dimensionality of a dataset that is considered to contain anisotropy effects, one should follow the original WAL criteria (Table 1), plus the new conditions described in Table 3. The exception is when the principal anisotropy directions are aligned with the measuring axes. In this situation, if the anisotropic media is 2D, the information contained in the induction arrows might be useful.

Another important point is that, except in very simple cases, the anisotropy cannot be identified from one site alone. It is fundamental to check for the consistency of dimensionality with neighbouring sites or periods.

Finally, the comparison of the dimensionality description obtained using the WAL invariant criteria with that from phase tensor diagrams allowed us to conclude that, in some cases, both provide the same information. However, when the phases do not change with period, such as in the case of an anisotropic half-space, only the WAL criteria enable the anisotropy to be identified. It is also important to note that in some cases the strike angle can only be computed from $\theta_{3D/2D}$, which considers the real and imaginary parts of the tensor, as opposed to the direction defined from the Mohr circles, θ_h, which uses the real or the imaginary parts separately.

Acknowledgements

The authors thank Ted Lilley for his critical review, which greatly helped improving the manuscript. We acknowledge Josef Pek for providing the 2D anisotropic forward code (Pek and Verner, 1997). This work has been funded by projects CGL2006-10166 and CGL2009-07604. A. Martí thanks the Universitat de Barcelona and the Department of Earth Sciences at Memorial University of Newfoundland (MUN) for facilitating her research term at MUN.

Appendix A.

In this Appendix A we first summarize the expressions used to compute the strike directions from the magnetotelluric tensor using Weaver et al. (2000) notation. Secondly, we derive these expressions for the theoretical magnetotelluric tensors corresponding to (A.2.1) a 2D isotropic structure, rotated an angle θ from the strike direction, and (A.2.2) an anisotropic half-space, with the main anisotropic directions rotated an angle α_S.

A.1. Strike expressions

The complex parameters $\varsigma_j = \xi_j + i \cdot \eta_j (j = 1, 4)$, are defined as linear combinations of the magnetotelluric tensor components: $\zeta_1 = (M_{xx} + M_{yy})/2$, $\zeta_2 = (M_{xy} + M_{yx})/2$, $\zeta_3 = (M_{xx} + M_{yy})/2$ and $\zeta_4 = (M_{xy} + M_{yx})/2$:

$$\underline{M} = \begin{pmatrix} M_{xx} & M_{xy} \\ M_{yx} & M_{yy} \end{pmatrix} = \begin{pmatrix} \zeta_1 + \zeta_3 & \zeta_2 + \zeta_4 \\ \zeta_2 - \zeta_4 & \zeta_1 - \zeta_3 \end{pmatrix} = \begin{pmatrix} \xi_1 + \xi_3 & \xi_2 + \xi_4 \\ \xi_2 - \xi_4 & \xi_1 - \xi_3 \end{pmatrix} + i \begin{pmatrix} \eta_1 + \eta_3 & \eta_2 + \eta_4 \\ \eta_2 - \eta_4 & \eta_1 - \eta_3 \end{pmatrix}. \quad \text{(A1)}$$

If the tensor corresponds to a 2D structure, the strike direction (θ_{2D}) can be computed from using either the real or the imaginary parts of ς_2 and ς_3, which lead to the same result: $\theta_{2D} = \theta_1 = \theta_2$:

$$\tan(2\theta_1) = -\frac{\xi_3}{\xi_2}. \quad \text{(A2)}$$

and:

$$\tan(2\theta_2) = -\frac{\eta_3}{\eta_2}. \quad \text{(A3)}$$

Both the ς_i parameters and the angles θ_1 and θ_2 can be represented in Mohr circle diagrams (for the real and imaginary parts), which are also used to represent WAL invariants (Fig. 1).

If the 2D structure is affected by galvanic distortion, the strike direction ($\theta_{3D/2D}$) can be recovered using the expression:

$$\tan(2\theta_{3D/2D}) = \frac{d_{12} - d_{34}}{d_{13} + d_{24}} \quad \text{(A4)}$$

where $d_{ij} = (\xi_i\eta_j - \xi_j\eta_i)/(I_1 I_2)$, and I_1 and I_2 are rotational invariants of the MT tensor.

Given that 2D is a particular case of 3D/2D (where the galvanic matrix is the identity), the same expression works to compute the strike, so that: $\theta_{2D} = \theta_1 = \theta_2 = \theta_{3D/2D}$.

A.2. Particular cases

A.2.1. 2D isotropic structure

$$\underline{M}_{2D} = \begin{pmatrix} 0 & M_{xy} \\ M_{yx} & 0 \end{pmatrix}, \tag{A5}$$

if the tensor is rotated an angle θ:

$$\underline{M'} = R_\theta \underline{M}_{2D} R_\theta^T = \begin{pmatrix} (M_{xy}+M_{yx})\sin\theta\cdot\cos\theta & M_{xy}\cos^2\theta - M_{yx}\sin^2\theta \\ -M_{xy}\sin^2\theta + M_{yx}\cos^2\theta & -(M_{xy}+M_{yx})\sin\theta\cos\theta \end{pmatrix}, \tag{A6}$$

and:

$$\begin{aligned} \zeta_1 &= 0 \\ \zeta_2 &= (M_{xy}+M_{yx})(\sin^2\theta - \cos^2\theta)/2 \\ \zeta_3 &= (M_{xy}+M_{yx})\sin\theta\cos\theta \\ \zeta_4 &= (M_{xy}-M_{yx})/2 \end{aligned}, \tag{A7}$$

$$\tan(2\theta_1) = -\frac{Re(M_{xy}+M_{yx})\sin\theta\cos\theta}{Re(M_{xy}+M_{yx})((\sin^2\theta-\cos^2\theta)/(2))} = -\frac{2\sin\theta\cos\theta}{\sin^2\theta-\cos^2\theta} = -\frac{\sin(2\theta)}{-\cos(2\theta)} = \tan(2\theta), \tag{A8}$$

and:

$$\tan(2\theta_2) = -\frac{Im(M_{xy}+M_{yx})\sin\theta\cos\theta}{Im(M_{xy}+M_{yx})((\sin^2\theta-\cos^2\theta)/(2))} = -\frac{2\sin\theta\cos\theta}{\sin^2\theta-\cos^2\theta} = -\frac{\sin(2\theta)}{-\cos(2\theta)} = \tan(2\theta). \tag{A9}$$

This proves that $\theta_{2D} = \theta_1 = \theta_2 = \theta$.

Using the expression in (A4):

$$d_{12} = d_{13} = 0,$$

$$d_{34} = \frac{(Re(M_{xy}+M_{yx}))\sin\theta\cos\theta(\mathrm{Im}(M_{xy}-M_{yx}))/(2) - (\mathrm{Re}(M_{xy}-M_{yx}))/(2)\mathrm{Im}(M_{xy}+M_{yx}))\sin\theta\cos\theta}{I_1 I_2},$$

$$d_{24} = \frac{(\mathrm{Re}(M_{xy}+M_{yx}))(\sin^2\theta-\cos^2\theta)/(2)(\mathrm{Im}(M_{xy}+M_{yx}))/(2) - (\mathrm{Re}(M_{xy}-M_{yx}))/(2)\mathrm{Im}(M_{xy}+M_{yx})((\sin^2\theta-\cos^2\theta)/(2))}{I_1 I_2}.$$

Hence:

$$\tan(2\theta_{3D/2D}) = \frac{-d_{34}}{d_{24}} = -2\frac{(\mathrm{Im}(M_{xy}+M_{yx})\mathrm{Re}(M_{xy}-M_{yx}) - \mathrm{Re}(M_{xy}+M_{yx})\mathrm{Im}(M_{xy}-M_{yx}))\sin\theta\cos\theta}{(\mathrm{Im}(M_{xy}+M_{yx})\mathrm{Re}(M_{xy}-M_{yx}) - \mathrm{Re}(M_{xy}+M_{yx})\mathrm{Im}(M_{xy}-M_{yx}))(\sin^2\theta-\cos^2\theta)}$$

$$= \frac{-2\sin\theta\cos\theta}{\sin^2\theta-\cos^2\theta} = \frac{-\sin(2\theta)}{-\cos(2\theta)} = \tan(2\theta),$$

which proves that:

$$\theta_{3D/2D} = \theta_1 = \theta_2 = \theta.$$

A.2.2. Anisotropic half-space

The analytic expression of the MT tensor corresponding to an anisotropic half-space, with the main anisotropic directions rotated an angle α_S is obtained using the development from Pek and Santos (2002):

$$\underline{M}_{\mathrm{anis}} = C\begin{pmatrix} d\sin(2\alpha_S) & -s - d\cos(2\alpha_S) \\ s - d\cos(2\alpha_S) & -d\sin(2\alpha_S) \end{pmatrix}(i+1),$$

where C is a constant, $s = \sqrt{\rho'_{xx}} + \sqrt{\rho'_{yy}}$ and $d = \sqrt{\rho'_{xx}} - \sqrt{\rho'_{yy}}$.

$$\begin{aligned} \zeta_1 &= 0 \\ \zeta_2 &= -C\frac{d}{2}\cos(2\alpha_S)(1+i) \\ \zeta_3 &= C\frac{d}{2}\sin(2\alpha_S)(1+i) \\ \zeta_4 &= Cs(1+i) \end{aligned}.$$

Given that both the real and imaginary parts have the same value:

$$\tan(2\theta_1) = \tan(2\theta_2) = -\frac{(d/2)\sin(2\alpha_S)}{-(d/2)\cos(2\alpha_S)} = \tan(2\alpha_S),$$

which proves that $\theta_{2D} = \theta_1 = \theta_2 = \alpha_S$.

On the other hand, if the strike direction is computed using the expression of $\theta_{3D/2D}$, $d_{ij} = 0$, for any i, j because real and imaginary parts of the tensor are identical. Consequently: $\tan(2\theta_{3D/2D}) = 0/0$, which is an undetermination.

References

Caldwell, T.G., Bibby, H.M., Brown, C., 2004. The magnetotelluric phase tensor. Geophys. J. Int. 158, 457–469.

Cantwell, T., 1960. Detection and analysis of low frequency magnetotelluric signals. Ph.D. Thesis, Dept. of Geology and Geophysics, M.I.T. Cambridge, MA.

Eaton, D.W., Jones, A.G., 2006. Tectonic fabric of the subcontinental lithosphere: evidence from seismic, magnetotelluric and mechanical anisotropy. Phys. Earth Planet. Inter. 158, 85–91.

Fischer, G., Masero, W., 1994. Rotational properties of the magnetotelluric impedance tensor, the example of the Araguainha impact crater, Brazil. Geophys. J. Int. 119, 548–560.

Gatzemeier, A., Tommasi, A., 2006. Flow and electrical anisotropy in the upper mantle: finite-element models constraints on the effects of olivine crystal preferred orientation and microstructure. Phys. Earth Planet. Inter. 158, 92–106.

Groom, R.W., Bailey, R.C., 1989. Decomposition of the magnetotelluric impedance tensor in the presence of local three-dimensional galvanic distortion. J. Geophys. Res. 94, 1913–1925.

Heise, W., Pous, J., 2003. Anomalous phases exceeding 90° in magnetotellurics: anisotropic model studies and a field example. Geophys. J. Int. 155, 308–318.

Heise, W., Caldwell, T.G., Bibby, H.M., Brown, C., 2006. Anisotropy and phase splits in magnetotellurics. Phys. Earth Planet. Inter. 158, 107–121.

Jones, A.G., 1993. The COPROD2 dataset: tectonic setting, recorded MT data and comparison of models. J. Geomagn. Geoelectr. 45, 933–955.

Jones, A.G., 2006. Electromagnetic interrogation of the anisotropic Earth: looking into the Earth with polarized spectacles. Phys. Earth Planet. Inter. 158, 281–291.

Jones, A.G., Craven, J.A., 1990. The North American Central Plains conductivity anomaly and its correlation with gravity, magnetics, seismic, and heat flow data in the Province of Saskatchewan. Phys. Earth Planet. Inter. 60, 169–194.

Jones, A.G., Craven, J.A., McNeice, G.A., Ferguson, I.J., Boyce, T., Farquharson, C., Ellis, R.G., 1993. The North American Central Plains conductivity anomaly within the Trans-Hudson orogen in northern Saskatchewan. Geology 21, 1027–1030.

Kaufman, A.A., 1988. Reduction of the geological noise in magnetotelluric soundings. Geoexploration 25, 145–161.

Li, Y., 2002. A finite-element algorithm for electromagnetic induction in two-dimensional anisotropic conductivity structures. Geophys. J. Int. 148, 389–401.

Lilley, F.E.M., 1993. Magnetotelluric analysis using Mohr circles. Geophysics 58, 1498–1506.

Lilley, F.E.M., 1998a. Magnetotelluric tensor decomposition. Part I. Theory for a basic procedure. Geophysics 63, 1885–1897.

Lilley, F.E.M., 1998b. Magnetotelluric tensor decomposition. Part II. Examples of a basic procedure. Geophysics 63, 1898–1907.

Lilley, F.E.M., Weaver, J.T., 2009. Phases greater than 90° in MT data: analysis using dimensionality tools. Journal of Applied Geophysics 70, 9–16.

Martí, A., Queralt, P., Roca, E., 2004. Geoelectric dimensionality in complex geologic areas: application to the Spanish Betic Chain. Geophys. J. Int. 157, 961–974.

Martí, A., Queralt, P., Ledo, J., 2009. WALDIM: a code for the dimensionality analysis of magnetotelluric data using the rotational invariants of the magnetotelluric tensor. Comp. Geosci. 35, 2295–2303.
McNeice, G., Jones, A.G., 2001. Multisite, multifrequency tensor decomposition of magnetotelluric data. Geophysics 66, 158–173.
Negi, J.G., Saraf, P.D., 1989. Anisotropy in Geoelectromagnetism. Methods in Geochemistry and Geophysics, vol. 28. Elsevier, Amsterdam.
Osella, A.M., Martinelli, P., 1993. Magnetotelluric response of anisotropic 2-D structures. Geophys. J. Int. 115, 819–828.
Pek, J., Santos, F.A.M., 2002. Magnetotelluric impedances and parametric sensitivities for 1-D anisotropic media. Comp. Geosci. 28, 939–950.
Pek, J., Santos, F.A.M., 2006. Magnetotelluric inversion for anisotropic conductivities in layered media. Phys. Earth Planet. Inter. 158, 139–158.
Pek, J., Verner, T., 1997. Finite-difference modelling of magnetotelluric fields in two-dimensional anisotropic media. Geophys. J. Int. 128, 505–521.
Reddy, I.K., Rankin, D., 1975. Magnetotelluric response of laterally inhomogeneous and anistotropic media. Geophysics 40, 1035–1045.
Saraf, P.D., Negi, J.G., Cerv, V., 1986. Magnetotelluric response of a laterally inhomogeneous anisotropic inclusion. Phys. Earth Planet. Inter. 43, 196–198.
Simpson, F., Bahr, K., 2005. Practical Magnetotellurics. Cambridge Univesity Press.
Smith, J.T., 1995. Understanding telluric distortion matrices. Geophys. J. Int. 122, 219–226.
Szarka, L., Menvielle, M., 1997. Analysis of rotational invariants of the magnetotelluric impedance tensor. Geophys. J. Int. 129, 133–142.
Vozoff, K., 1991. The magnetotelluric method. Electromagnetic Methods in Applied Geophysics, vol. 2. Applications. Soc. Expl. Geophys., Tulsa, OK.
Wang, T., Fang, S., 2001. 3-D electromagnetic anisotropy modeling using finite differences. Geophysics 66, 1386–1398.
Wang, D., Mookherjee, M., Xu, Y., Karato, S., 2006. The effect of water on the electrical conductivity of olivine. Nature 443, 977–980.
Wannamaker, P.E., 2005. Anisotropy versus heterogeneity in continental solid Earth electromagnetic studies: Fundamental response characteristics and implications for physicochemical state. Surv. Geophys. 26, 733–765.
Weaver, J.T., Agarwal, A.K., Lilley, F.E.M., 2000. Characterisation of the magnetotelluric tensor in terms of its invariants. Geophys. J. Int. 141, 321–336.
Weidelt, P., 1999. 3D conductivity models: implications of electrical anisotropy. In: Oristaglio, M., Spies, B. (Eds.), Three-Dimensional Electromagnetics. Society of Exploration Geophysicists, Tulsa, OK, pp. 119–137.
Yin, C., 2003. Inherent nonuniqueness in magnetotelluric inversion for 1D anisotropic models. Geophysics 68, 138–146.
Yoshino, T., Matsuzaki, T., Yamashita, S., Katsura, T., 2006. Hydrous olivine unable to account for conductivity anomaly at the top of the asthenosphere. Nature 443, 973–976.